Title
Collective Flow Measured with the Plastic Ball

Authors
Ritter, Hans G.
Gutbrod, H.H.
Kampert, K.H.
et al.

Publication Date
1989-08-01

LBL-27617

Lawrence Berkeley Laboratory
UNIVERSITY OF CALIFORNIA

Presented at the NATO Advanced Study Institute on the Nuclear Equation of State, Peñíscola, Spain, May 21–June 3, 1989

Collective Flow Measured with the Plastic Ball

H.G. Ritter, H.H. Gutbrod, K.H. Kampert, B. Kolb, A.M. Poskanzer, R. Schicker, H.R. Schmidt, and T. Siemiarczuk

August 1989

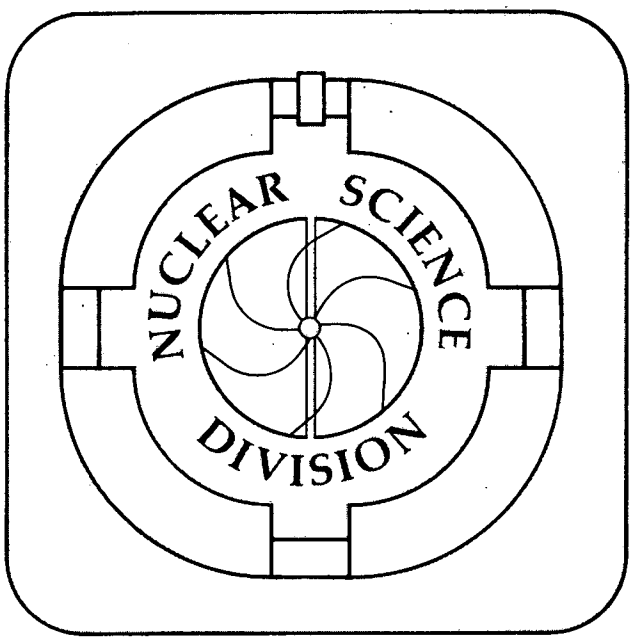

Prepared for the U.S. Department of Energy under Contract Number DE-AC03-76SF00098.

DISCLAIMER

COLLECTIVE FLOW MEASURED WITH THE PLASTIC BALL

H.G. Ritter, H.H. Gutbrod, K.H. Kampert, B. Kolb, A.M. Poskanzer, R. Schicker, H.R. Schmidt, and T. Siemiarczuk

Gesellschaft für Schwerionenforschung,
D-6900 Darmstadt, West Germany
and
Nuclear Science Division, Lawrence Berkeley Laboratory,
University of California, Berkeley, CA 94720, USA

INTRODUCTION

The study of the bulk properties of nuclear matter, *e.g.* the equation of state or the transport properties, is one of the main objectives of relativistic heavy ion physics. As pointed out many times during this conference, the knowledge of these properties is of fundamental interest and it is also essential for the understanding of supernova explosions and of the structure of neutron stars.

The collision of heavy ions has been described by many different approaches. Intranuclear cascade calculations are based on the assumption that a nuclear collision is equivalent to the superposition of nucleon-nucleon collisions. Hydrodynamical models on the other hand predicted the appearance of shock waves initiated by a very high energy incident particle early on [1] and other authors also considered shock waves in colliding nuclei [2, 3]. But a mechanism of shock compression in nucleus-nucleus collisions that would lead to densities 3 to 5 times higher than that of normal nuclear matter was first proposed by Scheid *et al.* [4].

A signature of the compression effects predicted by the calculations using a nontrivial equation of state is collective flow of the nuclear matter in the expansion phase [4, 5, 6]. Collective flow is the consequence of the pressure buildup in the high density zone through the short range repulsion between nucleons, *i.e.* through compressional energy. This effect leads to characteristic, azimuthally asymmetric sidewards emission of the reaction products.

Collective flow has not been observed in single particle inclusive measurements [7]. Early on a need was clearly seen for a large acceptance (4π) detector at the Bevalac. The Plastic Ball detector, which was designed to measure most of the charged particles from heavy ion reactions, is ideally suited to study the emission patterns and event shapes resulting from collective flow.

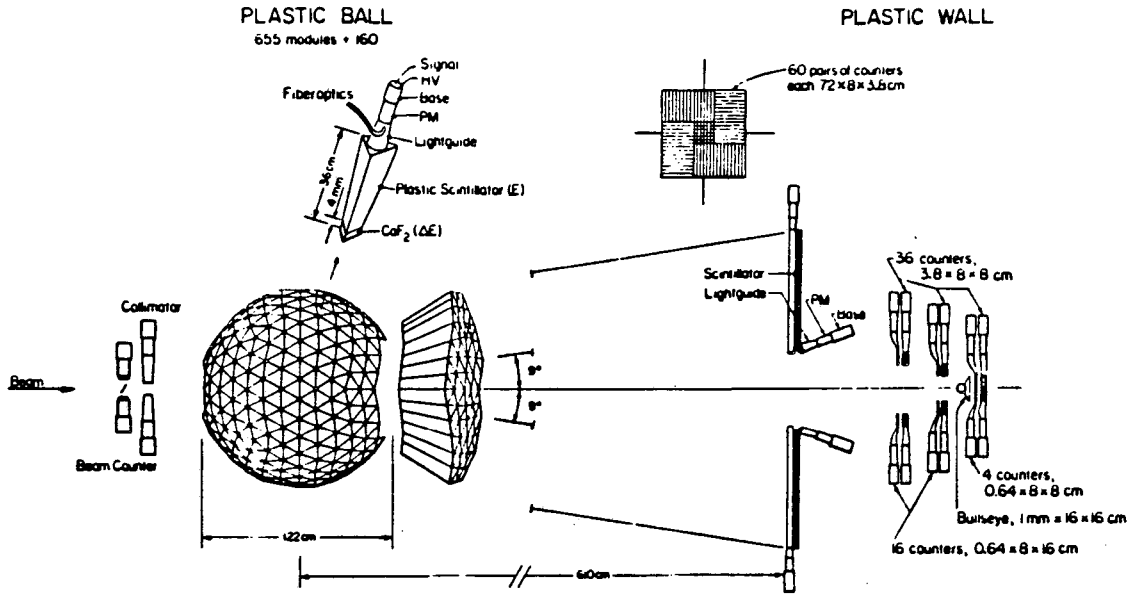

Figure 1: Schematic view of the Plastic Ball and the Plastic Wall. On the upper left is a picture of a single module and on the upper right is a view of the Wall as seen by the beam.

EXPERIMENT

For coverage of almost 4π the Plastic Ball was built completely surrounding the target except for the extreme backward angles, where the beam enters the system, and the extreme forward angles. Because of the large fragment velocities at forward angles the region from 0 to 10 deg was covered with a multielement time-of-flight system called the Plastic Wall. The complete system is shown schematically in Fig. 1 and described in detail in Ref. [8].

The Plastic Ball thus covers the region between 10 and 160 degrees, which is 96% of the total solid angle. It consists of 815 detectors where each module is a $\Delta E - E$ telescope capable of identifying the hydrogen and helium isotopes and positive pions. The ΔE measurement is performed with a 4 mm thick CaF_2 crystal and the E counter is a 36 cm long plastic scintillator. Both signals are read out by a single photomultiplier tube. Due to the different decay times of the two scintillators, ΔE and E information can be separated by gating two different ADCs at different times. Positive pions are additionally identified by measuring the delayed $\pi^+ \rightarrow \mu^+ \rightarrow e^+$ decay.

THE MULTIPLICITY PARAMETER

In measuring the proton multiplicity, N_p, we attempt to account for all participant protons, including those bound in light composites (d, t, ^{3}He, and ^{4}He). These bound protons add approximately 40% to the proton multiplicity. The proton energy threshold in the laboratory frame is approximately 15 MeV. The energy threshold for ions of charge 2 is roughly 2 or 3 times higher. The projectile spectators are largely eliminated by excluding a region in $p_\perp$-rapidity space that is identified by use of low multiplicity, peripheral events.

Since the particle multiplicity is related to the impact parameter, we classify the

events according to this proton multiplicity. The average multiplicity depends on the target-projectile mass and on the bombarding energy. To allow meaningful comparisons the multiplicity bins chosen should correspond always to approximately the same range in normalized impact parameter. The best approach is to divide the multiplicity distribution into bins of constant fractions of the maximum multiplicity. The multiplicity distribution has roughly the same form for all systems and energies: a monotonic decrease with increasing multiplicity with a rather pronounced plateau before the final sharp decrease at the highest multiplicities. Therefore the maximum multiplicity (N_p^{max}) can be defined at the point where the curve drops to one half the plateau height. Table 1 contains the value of $N_p^{max}/2Z$ for all symmetric systems measured. The data accumulated with a minimum bias trigger are then divided into 5 bins, 4 equal width bins between 0 and maximum multiplicity and one bin with multiplicities larger than N_p^{max}. These multiplicity bins are labelled MUL1, MUL2, MUL3, MUL4, and MUL5 and range from peripheral collisions with few observed charges to central collisions with very high multiplicities.

Table 1: Maximum participant proton multiplicities N_p^{max} divided by the sum of the projectile and target nuclear charges for all measured symmetric systems and beam energies.

E/A (MeV/A)	150	250	400	650	800	1050
Au + Au	0.41	0.58	0.71	0.81	0.85	
Nb + Nb	0.46	0.63	0.78	0.88	0.90	0.95
Ca + Ca			0.75			0.90

STOPPING AND THERMALIZATION

Obviously the use of the concept of bulk properties of nuclear matter needs experimental justification. We must prove that the system is in global, or at least local, thermal equilibrium. This has not yet been done rigorously, but with a 4π detector it is straightforward to measure the degree of stopping that can be reached in the reaction by investigating the rapidity distribution dN/dy of the baryons which is shown in Fig. 2 for Au + Au at 250 MeV per nucleon for three multiplicity bins. In peripheral reactions (top, MUL1) most of the reaction products experience a very small momentum transfer and stay at beam rapidity ($y = 0.72$) or at target rapidity ($y = 0$). However, since target rapidity fragments are absorbed in the target and cannot be observed in the detector, the distribution is not symmetric around midrapidity ($y = 0.36$). In semi-central collisions (Fig. 2 center, MUL3) already an appreciable amount of reaction products populates midrapidity. In central collisions (Fig. 2 bottom, MUL5) we observe a distribution that is symmetric around midrapidity. This indicates that the two Au nuclei completely stop each other and form a highly excited system at midrapidity.

More detailed information can be obtained by studying how the longitudinal momentum of the projectile is transformed into transverse motion during the collision. From the measured momenta of all the particles in the center of mass system we can calculate the ratio

$$R = \frac{2}{\pi} \sum_i \left| p_\perp^i \right| / \sum_i \left| p_{||}^i \right| . \qquad (1)$$

The sums in Eq. 1 contain the perpendicular, $p_\perp$, and longitudinal, $p_{||}$, momentum components of all particles in one event. Global stopping of the two nuclei in the center

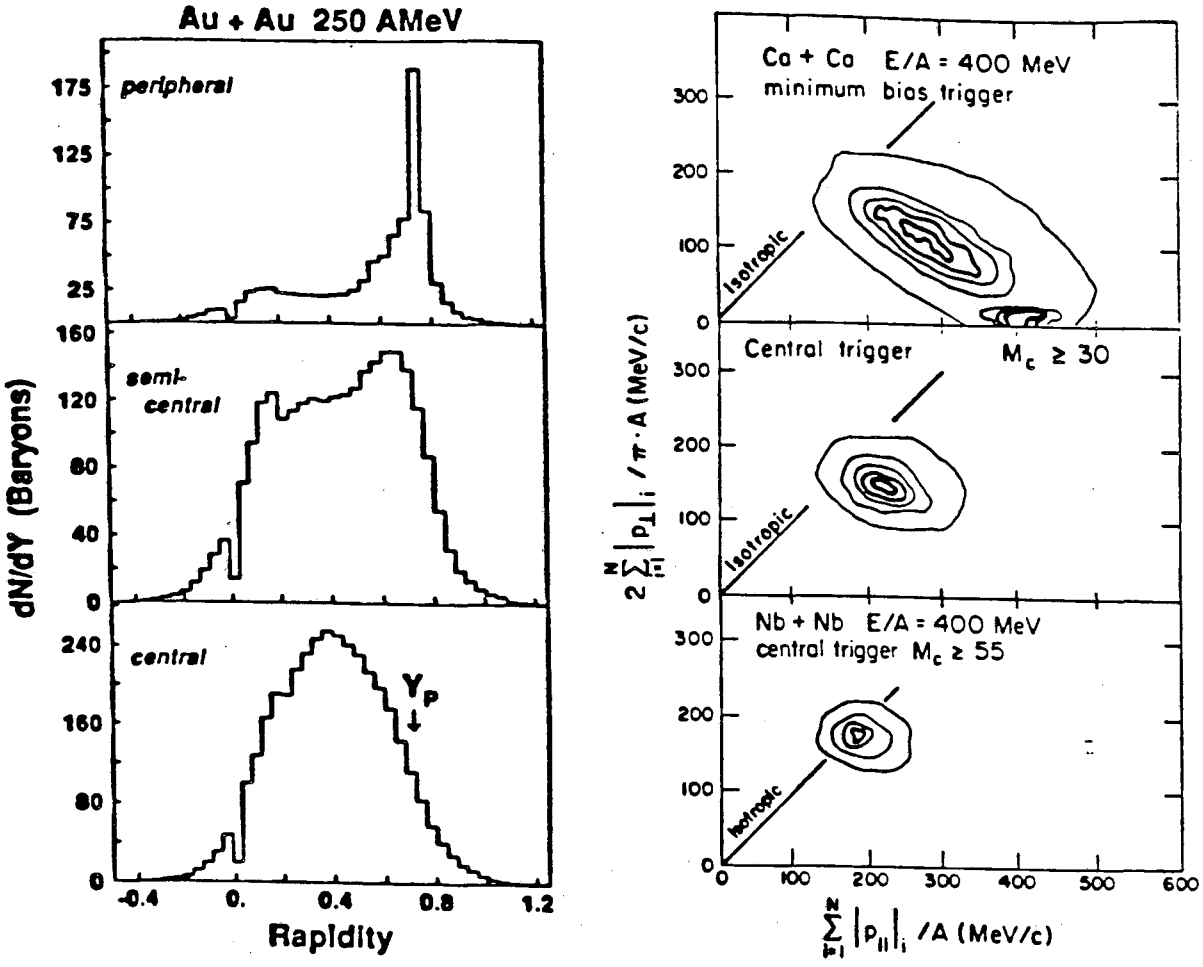

Figure 2: Baryon rapidity distributions for Au + Au collisions at 250 MeV per nucleon for three multiplicity bins. Baryons are defined as: $(1 + N/Z)n_p + 2n_d + 3(n_t + n_{^3He}) + 4(n_{^4He})$.

Figure 3: Contour plot of the average momentum components perpendicular and parallel to the beam axis for Ca + Ca (top and center) and Nb + Nb (bottom) at 400 MeV per nucleon. The diagonal line ($R = 1$) corresponds to isotropic events.

of mass system (or isotropic emission) would manifest itself by a ratio $R = 1$ [9]. Flow in the transverse direction would result in an even larger ratio. Thus, $R = 1$ is a necessary, but not sufficient condition, for thermalization. If in addition the energy distributions are of the Maxwell-Boltzmann type, the emitting system could be called thermalized.

The top part of Fig. 3 shows the yield as contour lines in the $p_\perp$-$p_{||}$ plane for minimum bias Ca + Ca events. The peak at small $p_\perp$ but large $p_{||}$ corresponds to peripheral reactions and is dominated by projectile fragments. This contribution vanishes if the trigger is changed to a central one. Figure 3 (center) shows central events with a charged particle multiplicity larger than 30. The maximum of the yield is shifted towards the diagonal line, calculated for isotropic emission, but only a few events actually reach $R = 1$, which in the limit of large multiplicity corresponds to full stopping of the two nuclei. In the lower part of Fig. 3 central events (charged particle multiplicity > 55) of Nb + Nb at 400 MeV per nucleon almost fulfill the stopping and isotropy condition ($R = 1$) on average. The multiplicity cuts applied correspond roughly to the same fraction of the total cross section for both systems. More quantitatively, R can be investigated as a function of multiplicity [10]. As expected from Fig. 3, R increases

with multiplicity and reaches a value of 0.62 for Ca, whereas it comes close to one for Nb. The increase with multiplicity can be explained by the decreasing role played by the projectile spectator particles as the collisions become more central. The difference between Ca and Nb central collisions may result because either Ca nuclei may be too small to stop each other at 400 MeV per nucleon or because stopping occurs only in the central part of the nuclear volume and surface effects are less important in Nb as compared with Ca.

ENERGY FLOW

The first attempt to determine the event shapes was done by adapting the thrust [5, 11, 12, 13] and sphericity [13, 14] analyses developed in high energy physics [15, 16] to the heavy ion case. The sphericity tensor

$$F_{ij} = \sum_{\nu} p_i(\nu) p_j(\nu) w(\nu)$$

is calculated from the momenta of all measured particles for each event. It is appropriate to chose the weight factor $w(\nu)$ so that composite particles have the same weight per nucleon as the individual nucleons of the composite particle at the same velocity. Commonly, the weight $w(\nu) = 1/2m(\nu)$ as proposed in Ref. [14] (kinetic energy flow) is used. Other coalescense invariant weights such as $1/p(\nu)$ [13] have been proposed and have been used in our analysis with similar results. The sphericity tensor approximates the event shape by an ellipsoid, whose orientation in space and whose aspect ratios can be calculated by diagonalizing the tensor.

The shapes predicted by hydrodynamical and intranuclear cascade calculations are quite different. The hydrodynamical model predicts prolate shapes along the beam axis for grazing collisions. With decreasing impact parameter the flow angle increases and reaches 90 degrees (with oblate shapes) for zero impact parameter events [5, 11, 12, 14]. This behaviour is independent of projectile and target mass. Early cascade calculations, however, predicted zero flow angles at all impact parameters [14]. Later, improved cascade calculations yielded finite, but small, flow angles [17, 18, 19].

Fluctuations due to finite particle effects are a major obstacle in extracting information from a flow analysis. Danielewicz and Gyulassy [20] have shown that those distortions strongly depend on multiplicity and that the flow angle Θ, if properly weighted by the Jacobian ($\sin\Theta$), is much less severely shifted towards higher values than the aspect ratios.

In this work the energy flow tensor [14] in the center of mass system has been determined and diagonalized for each individual event. The distribution of the flow angles (angle between the major axis of the flow ellipsoid and the beam axis) [21, 22] for Ca + Ca, Nb + Nb, and Au + Au at 400 MeV per nucleon is shown on the left side of Fig. 4 as a function of multiplicity. A striking difference between the light Ca system and the heavier Nb and Au systems can be observed. For all but the highest multiplicity bins, the distribution of the flow angles for the Ca data is peaked at 0 deg. For the heavier systems, however, there is a finite deflection angle increasing with increasing multiplicity. In addition, the flow angles increase with the mass of the system. An increase with mass has been predicted qualitatively by Vlasov-Uehling-Uhlenbeck calculations [23]; however, that predicted increase is more pronounced than the one observed here.

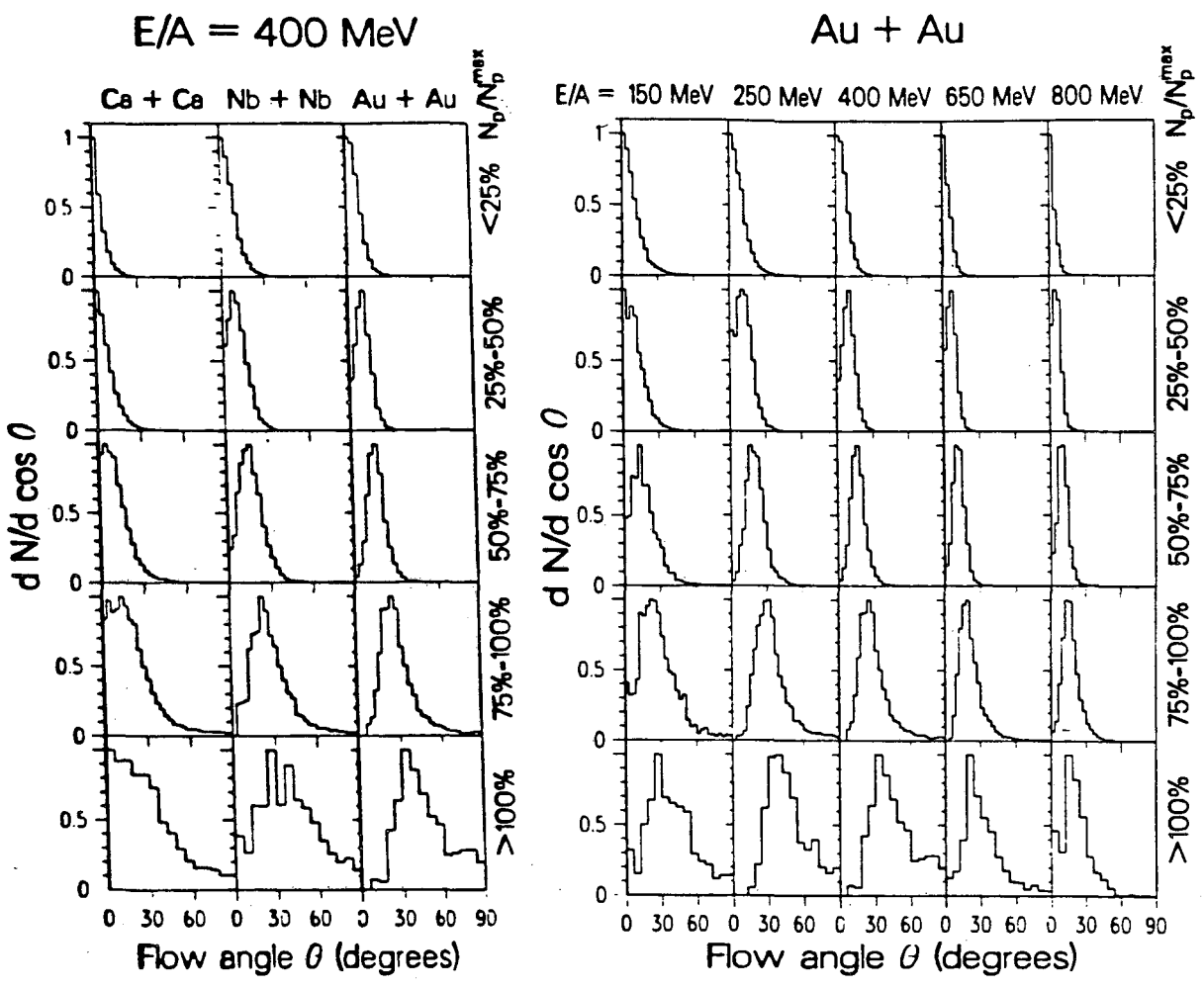

Figure 4: Distributions of the flow angles ($dN/d\cos\Theta$) in five multiplicity bins. The systems Ca + Ca, Nb + Nb, and Au + Au, all at 400 MeV per nucleon, are shown on the left, Au + Au at five energies is on the right.

Also important is the energy dependence of the flow angles. This is shown on the right side of Fig. 4 for five Au + Au energies from 150 MeV per nucleon up to 800 MeV per nucleon. The general trend observed is that the flow angles decrease with increasing energy above 250 MeV per nucleon. At the lowest energy the reaction mechanism responsible for the flow effect might lose importance in favor of other mechanisms known from low energy heavy ion reactions, such as, *e.g.*, deep inelastic scattering.

The decrease in the flow angles with increasing energy does not indicate that the flow effect gets smaller; it means, however, that the mean transverse momentum does not increase quite as fast as the longitudinal momentum. On the contrary, the mean perpendicular momentum transfer increases with energy, as will be seen from the transverse momentum analysis described in the next section.

So far, the events have been parameterized by ellipsoids, but it is of interest to study the shape in more detail. The presence of finite flow angles in the data indicates that in those events a reaction plane exists that is defined by the flow axis and the beam axis. All events can be rotated by the azimuthal angle ϕ, determined by the flow analysis, so that their individual reaction planes all fall into the x-z plane, with the z-axis being the beam axis. For those rotated events the invariant cross section in the reaction plane $d^2\sigma/dy\ d(p_x/m)$ [5, 11, 24] can be plotted, where p_x is the projection of the perpendicular

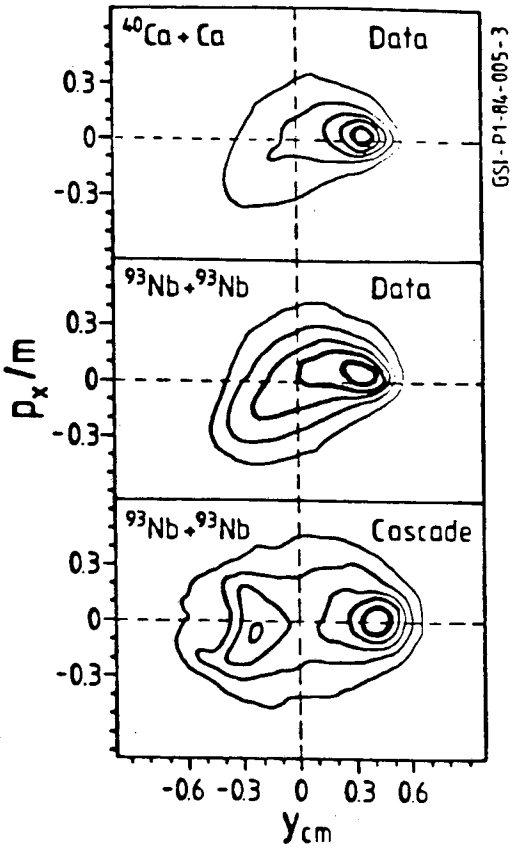

Figure 5: Contour plots (linear contours) of p_x/m as a function of the center of mass rapidity for multiplicities from 40 to 49 for Nb and 20 to 24 for Ca at 400 MeV per nucleon.

momentum into the reaction plane and y is the center of mass rapidity. Figure 5 shows this plot for a selected multiplicity bin for 400 MeV per nucleon Ca + Ca and Nb + Nb data, together with filtered events from a cascade code calculation [25]. The depletion near target rapidities is due to limited experimental acceptance for low energy particles in the laboratory system. This depletion enhances the flow angles artificially but does not change the reaction plane. The cascade plot is almost symmetric around the beam axis, whereas the Ca and Nb in-plane data plots are clearly asymmetric. The highest level contour results largely from the projectile remnants and indicates a definite bounce-off effect. The multiplicity dependence of the outer contour lines seems to follow the trend indicated by the flow angle distributions (Fig. 4). However, the position of the peak from the projectile remnants changes only slightly with multiplicity. Thus one can conclude that the strong sideward peaking (side-splash) seen in Fig. 4 is mainly due to the midrapidity particles. It should be noted that the bounce-off and side-splash effects are in the same plane.

The first report on the observation of finite flow angles by the Plastic Ball group [21] has been taken as proof for the existence of collective flow in relativistic heavy ion reactions [21, 24] and has stimulated, not only new experimental work and new analysis methods, but also new theoretical approaches.

TRANSVERSE MOMENTUM ANALYSIS

We have seen that the sphericity method is an extremely useful tool for establishing experimentally the existence of collective flow effects. However, reducing all the information available for each event to essentially one observable, the flow angle Θ, is a rather inclusive representation of the data. The contour plots of p_x/A versus y_{cm}, shown in Fig. 5, however, are very much influenced by experimental biases and are difficult to describe. Based on the observation that the reaction plane can also be determined from the collective transverse momentum transfer [26, 27], Danielewicz and Odyniec have proposed a better, more exclusive way to analyze the momentum contained in directed sidewards emission [27]. They propose presenting the data in terms of the mean transverse momentum per nucleon in the reaction plane $< p_x/A >$ as a function of the rapidity. By also removing autocorrelation effects this method is sensitive to the true dynamic correlations and has lead to indications for collective flow in cases where the kinetic energy flow analysis was not sensitive enough [27, 28]. Studying the momentum transfer as a function of rapidity permits one to distinguish between participant and spectator contributions and to exclude regions with large detector bias.

In the transverse momentum analysis the reaction plane is determined by the vector $\vec{Q}$ calculated for each event from the transverse momentum components $p_\perp$ of all the particles observed in the forward and backward hemispheres in the center of mass

$$\vec{Q} = \sum_i p_{\perp i}^{forw} - \sum_i p_{\perp i}^{back}.$$

Pions are not included. A similar method, using the transverse momentum unit vectors of the slow and fast particles was developed in parallel [26]. Each event can be rotated around the beam axis (z-axis) so that $\vec{Q}$ defines the x-axis of a new coordinate system. Autocorrelations are removed by calculating $\vec{Q}$ individually for each particle without including that particle. Evidently $\vec{Q}$ is only an estimate for the true reaction plane, and the projections into the estimated plane are too small by a factor $1/ < \cos\phi >$, where ϕ is the angle between the estimated and the true plane. The quantity $< \cos\phi >$ can be estimated [27] by randomly dividing the events into two subevents and averaging the cosine of one half the angle between the $\vec{Q}$ vectors of the two subevents.

Figure 6 shows the mean transverse momentum per nucleon projected into the reaction plane, $< p_x/A >$, as a function of the normalized center of mass rapidity, y/y_{proj}, for the third multiplicity bin (MUL3) of Nb + Nb collisions at a bombarding energy of 400 MeV per nucleon. The error bars reflect statistical errors only, and data points are corrected for the deviation from the true reaction plane, as described above. The curve exhibits the typical S-shape behavior demonstrating the dynamical collective momentum transfer between the forward and backward hemispheres.

It is our aim to extract quantitative information, with as little detector bias as possible, from the type of data presented in Fig. 6, thus allowing us to compare different mass systems at different beam energies with each other and with theoretical model calculations. The maximum transverse momentum transfer occurs close to the target and projectile rapidities, where there is great sensitivity to the exclusion of spectator particles and where the experimental biases are most disturbing. Therefore, the maximum value is not a good choice. However, to a good approximation, all curves are straight lines near midrapidity. If the data are plotted as a function of the normalized rapidity, the slope at midrapidity, which we call flow, has the dimensions of MeV/c per nucleon and is a measure of the amount of collective transverse momentum transfer in

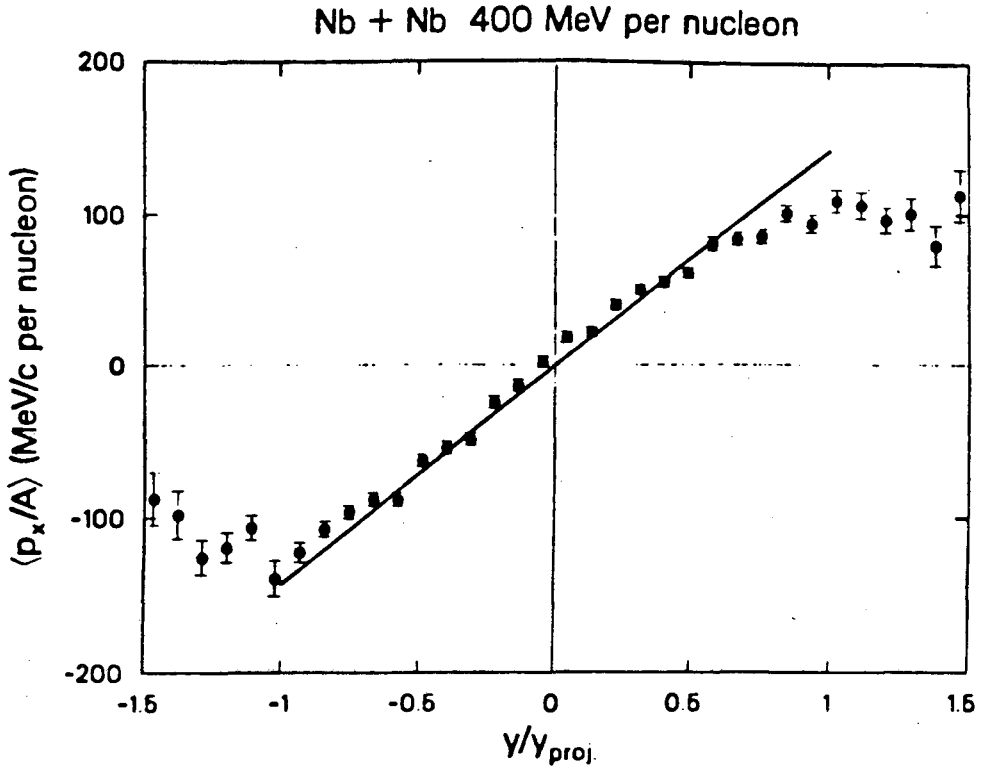

Figure 6: $< p_x/A >$ as a function of the normalized center of mass rapidity for 400 MeV per nucleon Nb + Nb in the third multiplicity bin. The slope of the solid line represents the flow obtained from fitting the data.

the reaction. Since the flow is determined at midrapidity it is a characteristic of the participants. Technically it is obtained by fitting a polynomial with first and third order terms to the S-shaped curve. The fit was done for y/y_{proj} between -1 and 1. Due to detector biases the curve is not completely symmetric about the origin; therefore a second order term has been included in the fit in cases where χ^2 can be improved considerably, as is the case for the higher energies and the heavier mass systems. The coefficient of the first order term, which is the slope of the fitted curve at $y/y_{proj} = 0$, is the flow. The straight line in Fig. 6 shows the result of this fit.

In Fig. 7 the flow, extracted from this kind of fits, is plotted as a function of the multiplicity for the three systems Ca + Ca, Nb + Nb, and Au + Au, all at a beam energy of 400 MeV per nucleon. As already seen from the distributions of the flow angle (see Fig. 4) [22], the amount of flow increases with increasing target-projectile mass. The multiplicity dependence, however, shows the flow peaking at intermediate multiplicity, whereas the mean flow angle increases monotonically with multiplicity (see Fig. 4) [21]. This is because the flow quantity goes to zero at zero impact parameter.

The multiplicity dependence shows a maximum in the directed flow between the third and fourth multiplicity bins. The mean value of the flow in these two multiplicity bins is shown in Fig. 8 as a function of the beam energy for all systems investigated. The flow increases monotonically with increasing beam energy — increasing rather rapidly up to about 400 MeV per nucleon and leveling off at the highest bombarding energies. The error bars represent statistical errors only. If in Fig. 8 the multiplicity averaged flow would be plotted instead of the maximum, then one would find a slight fall-off at beam energies above 650 MeV per nucleon, as reported in Ref. [29]. This difference is mainly due to the increasing contribution of peripheral reactions.

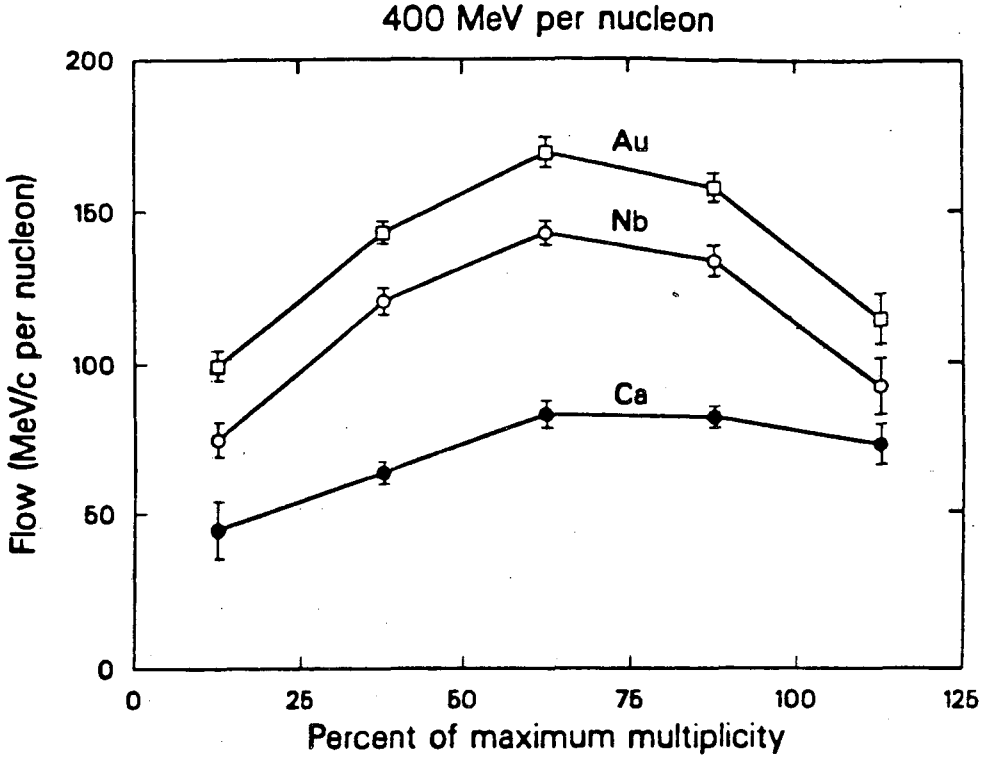

Figure 7: Flow as a function of the normalized participant proton multiplicity (N_p/N_p^{max}) for the three systems measured at a beam energy of 400 MeV per nucleon.

A different approach to analyzing the same data is to investigate multiparticle correlations globally between forward and backward hemispheres [30] in the center of mass system. This method also shows a peaking of the correlation function in semicentral collisions and a maximum value at 650 MeV per nucleon if integrated over multiplicity.

The transverse momentum transfer has been predicted by microscopic theories [31, 32] and by viscous fluid dynamics calculations [33]. Simpler models, like *e.g.* ideal fluid dynamics, cascade models, or fireball models, do not describe the data [34]. The microscopic theories [35] show a dependence of the flow on the nuclear matter equation of state. But the flow effects depend as well on the effective nucleon-nucleon cross sections which are not known. However, it might be possible to determine the effective cross sections from a systematic study of the nuclear stopping power via the dN/dy distributions [36] shown *e.g.* in Fig. 2. Once the cross sections are known, it should be possible to gain information about the equation of state from the flow effects.

TRIPLE DIFFERENTIAL CROSS SECTIONS

Over the last years we have seen a tremendous progress on the part of theoretical predictions. Many new microscopic models, all containing information about the equation of state, have been developed. The numerous contributions to this conference provide an excellent overview of this exciting development. Those models have greatly enhanced predictive power, and more quantitative comparisons between experimental results and these calculations will be needed. The comparisons will be done mainly in terms of triple differential cross sections [11]. A possibility for such a comparison is presented in Fig. 9. Here the yield, not yet the cross section, for proton emission into two differently defined cones is shown as a function of the center of mass energy of the protons for Nb + Nb

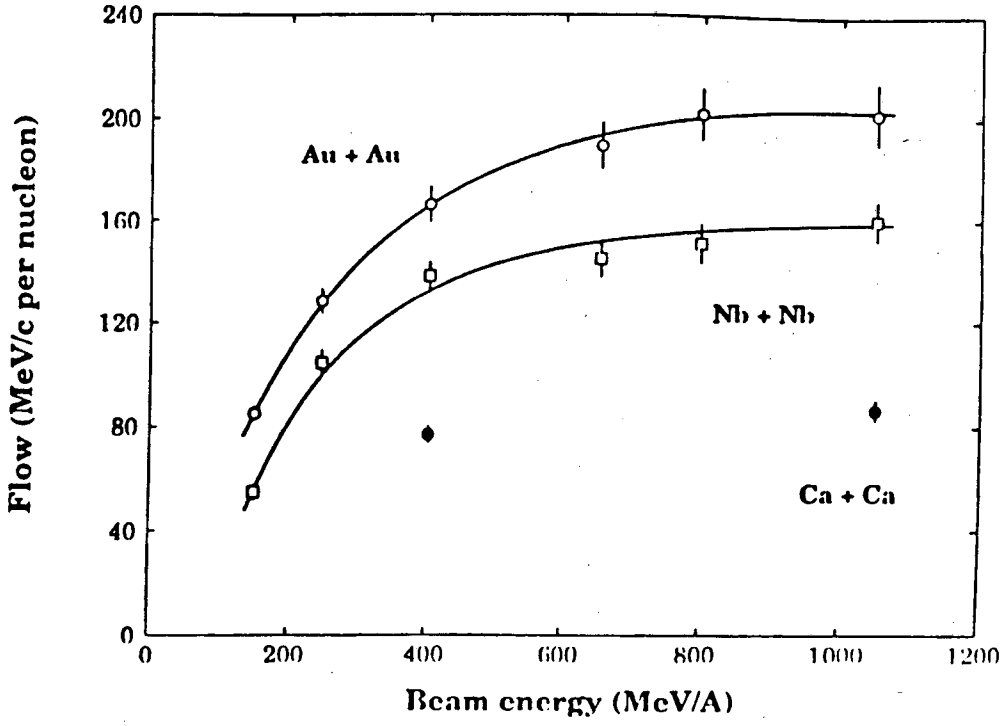

Figure 8: Flow of semicentral collisions ($50\% \leq N_p/N_p^{max} < 100\%$) as a function of beam energy.

at 400 MeV per nucleon. Only events with a flow angle between 35 deg and 55 deg have been selected, and only protons emitted into a cone around the flow axis (filled circles) and into a cone rotated by $\phi = 180$ deg (open circles) have been taken into account. This particular representation has the advantage that the protons emitted into the two cones have the same laboratory angle, thus minimizing acceptance problems. It can be clearly seen that more particles are emitted in the direction of the flow axis and that those protons on average have a higher momentum.

SUMMARY

In summary, the experimental results from the Plastic Ball detector have contributed vastly to the understanding of the reaction mechanism of nuclear collisions at several hundred MeV per nucleon. The discovery of the collective flow phenomena (bounce-off of spectator fragments, side-splash in the reaction plane, and squeeze-out out of the reaction plane described in Ref. [37]), as they were predicted by hydrodynamical models, has lead to the experimental observation of compressed nuclear matter, which is a necessary condition before one can study the equation of state in detail and search for phase transitions at higher energies.

Stimulated in part by the experimental successes, we have seen a tremendous progress on the theoretical side. There are many new microscopic models with greatly enhanced predictive power. In order to discriminate between different models and to extract more precise information about the nuclear equation of state, a comprehensive comparison with a large body of quantitative data will be necessary. It is expected that these data will mainly come from the new 4π detectors presently under construction at the new SIS/ESR accelerator at GSI [38] and at the Bevalac [39]. This will surely lead to a better understanding of the bulk properties of nuclear matter.

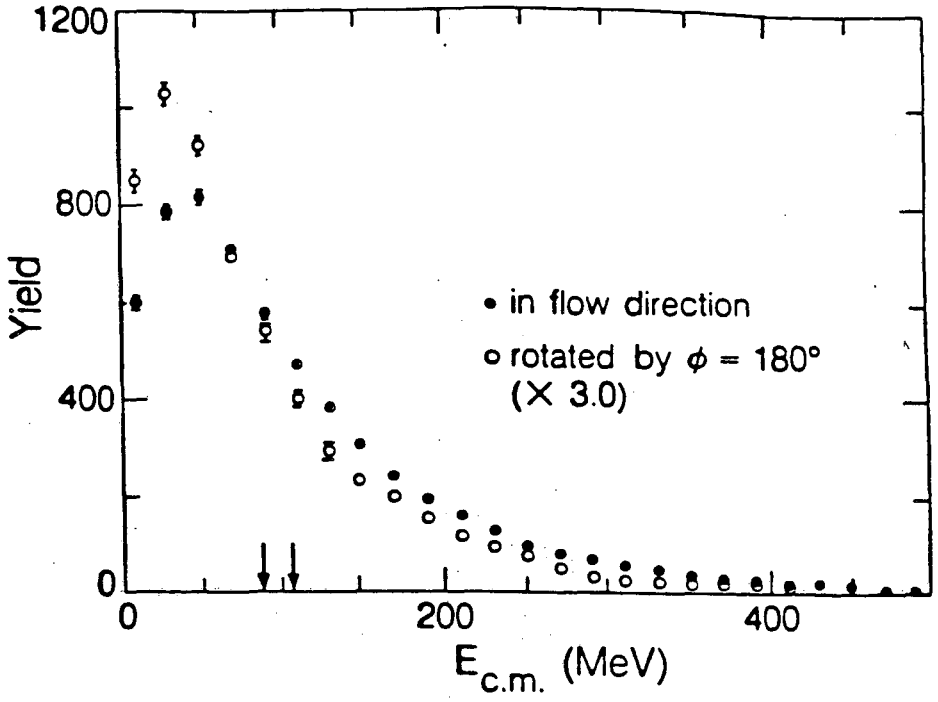

Figure 9: Energy spectra of protons emitted into a cone along the flow axis (filled circles) and into a cone rotated by $\phi = 180$ deg (open circles) for events with flow angles between 35 deg and 55 deg.

Acknowledgement
HGR would like to thank Prof. W. Greiner and Prof. H. Stöcker for the invitation to this exciting and stimulating conference. This work was supported by the Director, Office of Energy Research, Office of High Energy and Nuclear Physics, Division of Nuclear Physics of the U.S. Department of Energy under Contract DE-AC03-76SF00098.

References

[1] A.E. Glassgold, W. Heckrotte, and K.M. Watson, Ann. Phys. (NY) 6, 1 (1959).
[2] G.F. Chapline, M.H. Johnson, E. Teller, and M.S. Weiss, Phys. Rev. D8, 4302 (1973).
[3] M.I. Sobel, P.J. Siemens, J.P. Bondorf, and H.A. Bethe, Nucl. Phys. A251, 502 (1975).
[4] W. Scheid, H. Müller, W. Greiner, Phys. Rev. Lett. 32, 741 (1974).
[5] H. Stöcker, J. Hofmann, J.A. Maruhn, and W. Greiner, Progr. in Part. and Nucl. Phys. Vol.4, 133 (1980).
[6] H. Stöcker and W. Greiner, Phys. Reports 137, 277 (1986).
[7] A.M. Poskanzer, these Proceedings.
[8] A. Baden, H.H. Gutbrod, H. Löhner, M.R. Maier, A.M. Poskanzer, T. Renner, H. Riedesel, H.G. Ritter, H. Spieler, A. Warwick, F. Weik, and H. Wieman, Nucl. Instr. and Meth. 203, 189 (1982).
[9] H. Ströbele, R. Brockmann, J.W. Harris, F. Riess, A. Sandoval, R. Stock, K.L. Wolf, H.G. Pugh, L.S. Schroeder, R.E. Renfordt, K. Tittel, and M. Maier, Phys. Rev. C27, 1349 (1983).

[10] H.Å. Gustafsson, H.H. Gutbrod, B. Kolb, H. Löhner, B. Ludewigt, A.M. Poskanzer, T. Renner, H. Riedesel, H.G. Ritter, A. Warwick, and H. Wieman, Phys. Lett. B142, 141 (1984).
[11] H. Stöcker, L.P. Csernai, G. Graebner, G. Buchwald, H. Kruse, R.Y. Cusson, J.A. Maruhn, and W. Greiner, Phys. Rev. C25, 1873 (1982).
[12] J. Kapusta and D. Strottman, Phys. Lett. B106, 33 (1981).
[13] J. Cugnon, J. Knoll, C. Riedel, and Y. Yariv, Phys. Lett. B109, 167 (1982).
[14] M. Gyulassy, K.A. Frankel, and H. Stöcker, Phys. Lett. B110, 185 (1982).
[15] S. Brandt and H.D. Dahmen, Z. Physik C1, 61 (1979).
[16] S.L. Wu and G. Zoberning, Z. Physik C2, 107 (1979).
[17] J. Cugnon and D. L'Hôte, Nucl. Phys. A447, 27c (1985).
[18] J.J. Molitoris, H. Stöcker, H.Å. Gustafsson, J. Cugnon, D. L'Hôte, Phys. Rev. C33, 867 (1986).
[19] E. Braun and Z. Fraenkel, Phys. Rev. C34, 120 (1986).
[20] P. Danielewicz and M. Gyulassy, Phys. Lett. B129, 283 (1983).
[21] H.Å. Gustafsson, H.H. Gutbrod, B. Kolb, H. Löhner, B. Ludewigt, A.M. Poskanzer, T. Renner, H. Riedesel, H.G. Ritter, A. Warwick, F. Weik, and H. Wieman, Phys. Rev. Lett. 52, 1590 (1984).
[22] H.G. Ritter, K.G.R. Doss, H.Å. Gustafsson, H.H. Gutbrod, K.H. Kampert, B. Kolb, H. Löhner, B. Ludewigt, A.M. Poskanzer, A. Warwick, and H. Wieman, Nucl. Phys. A447, 3c (1985).
[23] J.J. Molitoris, D. Hahn, and H. Stöcker, Nucl. Phys. A447, 13c (1985).
[24] G. Buchwald, G. Graebner, J. Theis, J. Maruhn, W. Greiner, and H. Stöcker, Phys. Rev. Lett. 52, 1594 (1984).
[25] Y. Yariv and Z. Fraenkel, Phys. Rev. C20, 2227 (1979).
[26] H.Å. Gustafsson, H.H. Gutbrod, B. Kolb, H. Löhner, B. Ludewigt, A.M. Poskanzer, T. Renner, H. Riedesel, H.G. Ritter, T. Siemiarczuk, J. Stepaniak, A. Warwick, and H. Wieman, Z. Physik A321, 389 (1985).
[27] P. Danielewicz and G. Odyniec, Phys. Lett. B157, 146 (1985).
[28] D. Beavis, S.Y. Fung, W. Gorn, D. Keane, Y.M. Liu, R.T. Poe, G. VanDalen, and M. Vient, Phys. Rev. Lett. 54, 1652 (1985).
[29] K.G.R. Doss, H.Å. Gustafsson, H.H. Gutbrod, K.H. Kampert, B. Kolb, H. Löhner, B. Ludewigt, A.M. Poskanzer, H.G. Ritter, H.R. Schmidt, and H. Wieman, Phys. Rev. Lett. 57, 302 (1986).
[30] P. Beckmann, K.G.R. Doss, H.Å. Gustafsson, H.H. Gutbrod, K.H. Kampert, B. Kolb, H. Löhner, A.M. Poskanzer, H.G. Ritter, H.R. Schmidt, T. Siemiarczuk, and H. Wieman, Modern Phys. Lett. A2, 169 (1987).
[31] J.J. Molitoris and H. Stöcker, Phys. Lett. B162, 47 (1985).
[32] J.J. Molitoris, H. Stöcker, and B.L. Winer, Phys. Rev. C36, 220 (1987).
[33] G. Peilert, A. Rosenhauer, T. Rentsch, H. Stöcker, J. Aichelin, and W. Greiner, Proceedings of the 8th High Energy Heavy Ion Study, page 43, LBL-24580 (1988).
[34] B. Schürmann and W. Zwermann, Phys. Rev. Lett. 59, 2848 (1987).
[35] G. Peilert, H. Stöcker, W. Greiner, A. Rosenhauer, A. Bohnet, and J. Aichelin, Phys. Rev. C39, 1402 (1989).
[36] M. Berenguer, C. Hartnack, G. Peilert, A. Rosenhauer, W. Schmidt, J. Aichelin, J.A. Maruhn, W. Greiner, and H. Stöcker, Preprint UFTP-228 (1989).
[37] K.H. Kampert et al., these Proceedings.
[38] P. Kienle, these Proceedings.
[39] G. Rai et al., these Proceedings.

LAWRENCE BERKELEY LABORATORY
TECHNICAL INFORMATION DEPARTMENT
1 CYCLOTRON ROAD
BERKELEY, CALIFORNIA 94720